

Thermal Transport in Au-Core Polymer-Shell Nanoparticles

Zhenbin Ge,^{*,†} Youngjong Kang,[‡] T. Andrew Taton,[‡] Paul V. Braun,[†] and David G. Cahill[†]

Department of Materials Science and Engineering, the Frederick Seitz Materials Research Laboratory, and the Beckman Institute for Advanced Science and Technology, University of Illinois, Urbana, Illinois 61801, and Department of Chemistry, University of Minnesota, 207 Pleasant St SE, Minneapolis, Minnesota 55455

Received December 12, 2004; Revised Manuscript Received January 19, 2005

ABSTRACT

Thermal transport in aqueous suspensions of Au-core polymer-shell nanoparticles is investigated by time-resolved measurements of optical absorption. The addition of an organic cosolvent to the suspension causes the polystyrene component of the polymer shell to swell, and this change in the microstructure of the shell increases the effective thermal conductivity of the shell by a factor of approximately 2. The corresponding time scale for the cooling of the nanoparticle decreases from 200 ps to approximately 100 ps. The threshold concentration of cosolvent that creates the changes in thermal conductivity, 5 vol % tetrahydrofuran in water or 40 vol % *N,N*-dimethylformamide in water, is identical to the threshold concentrations for producing small shifts in the frequency of the plasmon resonance. Because the maximum fraction of solvent in the polymer shell is less than 20 vol %, the increase in the effective thermal conductivity of the shell cannot be easily explained by contributions to heat transport by the solvent or enhanced alignment of the polystyrene backbone along the radial direction.

Metal nanoparticles have been proposed as targeted thermal agents for use in medical therapies and drug delivery^{1–4} and could extend the precision of thermal effects below cellular dimensions.⁴ Gold nanoparticles are leading candidate materials for these applications because of their biocompatibility and because well-developed surface chemistries are available to functionalize Au nanoparticles for attachment to selected biological molecules or materials. The optical properties of Au nanoparticles can also be optimized by layered structures; for example, a dielectric nanoparticle surrounded by a Au shell has a large absorption coefficient in the near-infrared where biological tissues are relatively transparent, and high power diode lasers provide an efficient and convenient heat source.^{2,3}

Time-resolved measurement of optical absorption using ultrafast lasers has proven to be a flexible and powerful technique for probing heat transport within suspensions of metal nanoparticles;^{5–7} a pump laser beam is used to heat the nanoparticles, and a time-delayed probe beam monitors changes in the imaginary part of the index of refraction of the suspension. Many research groups have studied how the environment of a nanoparticle affects the decay of the particle

temperature,^{7–10} but these data, in most cases, have not been analyzed quantitatively to extract information about the thermophysical properties or microstructure of the material surrounding the nanoparticle. A notable exception is the recent work by Hartland and co-workers: heat transport in suspensions of Au-core silica-shell nanoparticles revealed that heat transport in the silica shell depends on the composition of the solvent; i.e., solvent penetration into the porous silica shell changed the thermal conductivity of the shell significantly.¹¹

In our previous work, we emphasized the role of the nanoparticle/surfactant/fluid interfaces on thermal transport from nanoparticles to the surrounding fluid.^{6,12} In aqueous suspensions, these interface effects are relatively weak because the thermal conductance of the nanoparticle/water interface is large.¹² In this letter, we concentrate on measurements of the effective thermal conductivity of a polymer shell surrounding a Au nanoparticle.¹³ In contrast to our previous work on nanoparticle suspensions, where the cooling rate of the bare nanoparticle is always slower than predicted based on the bulk properties of the surrounding fluid, the cooling rate of these Au-core polymer-shell nanoparticles can be much faster than expected.

Au-core polymer-shell nanoparticles were synthesized by a recently reported method in which block copolymer

* Corresponding author. Tel: 1-217-244-8107; Fax: 1-217-333-2736; e-mail: zge@uiuc.edu

[†] University of Illinois.

[‡] University of Minnesota.

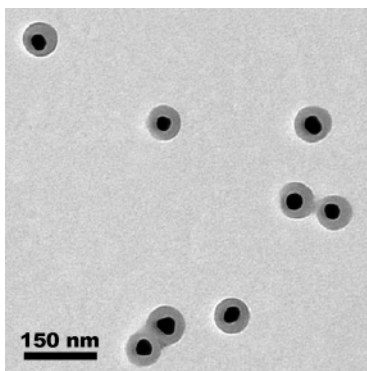


Figure 1. TEM images of Au nanoparticles encapsulated with PS₁₀₀-*b*-PAA₁₃ micelles dried from pure water. The diameter of the Au core is 31 ± 3 nm and the polymer shell is 16 ± 2 nm thick.

surfactant micelles are assembled around bare nanoparticles and then permanently fixed by chemical cross-linking of the copolymer.¹³ In this study, amphiphilic poly(styrene-*block*-acrylic acid) (PS₁₀₀-*b*-PAA₁₃) copolymer¹⁴ and dodecanethiol-capped Au nanoparticles ($d = 31 \pm 3$ nm)¹⁵ were initially dissolved together in *N,N*-dimethylformamide (DMF), a good solvent for both the hydrophobic (PS) and hydrophilic (PAA) polymer blocks and the nanoparticles. Gradual addition of water to this mixture induced the formation of a surfactant micelle around each nanoparticle. These Au-core micelle-shell structures were then made permanent by cross-linking the polyacrylate block of the micelles with 2,2'-(ethylene-dioxy)bis(ethylamine) and 1-(3-dimethylaminopropyl)-3-ethylcarbodiimide methiodide in water, as previously described.¹⁴ Transmission electron microscopy (TEM) images of the resulting nanoparticles dried from aqueous suspension show that each micelle shell contains exactly one nanoparticle and has uniform thickness, see Figure 1. Assuming that the two copolymer blocks segregate strongly in water, the highly asymmetric PS₁₀₀-*b*-PAA₁₃ copolymer forms a glassy shell that is composed almost entirely of polystyrene, which is further surrounded by a thin layer of cross-linked polyacrylate. We assume that the polyacrylate is on the outside of the polymer shell because the system is in water and the polyacrylate block is hydrophilic. This assumption is further supported by NMR data on encapsulated nanotubes,¹⁶ which show that the polyacrylate block is solvated in water and the polystyrene block is not. This cross-linked layer ensures that, as the polystyrene shell swells or desolvates in response to changes in the surrounding solvent, the polymer layer does not dissociate from the particle surface and the particles do not precipitate from suspension. For example, exposure of Au-core PS-shell particles to 20% tetrahydrofuran (THF) makes the shell permeable and exposes the particle core to chemical attack.¹³ It also turns the glassy PS shell fluid, as demonstrated by TEM images of core-shell particles before and after exposure to solvent.¹⁷

We use cooling rate of a nanoparticle heated by an ultrafast optical pulse to determine the thermal conductivity of the polymer shell. Transient absorption data are collected using a mode-locked Ti:sapphire laser that produces a series of <0.5 ps pulses at a repetition rate of 80.6 MHz. The laser

output is split into a “pump” beam whose optical path length is adjusted via a mechanical delay stage and whose intensity is modulated by an electrooptic modulator and a “probe” beam which is modulated by a mechanical chopper. We use pump and probe beam powers of 10–15 mW, a wavelength of 770 nm, and a $1/e^2$ beam radius of $8 \mu\text{m}$. The differences in transmitted probe intensity caused by the pump pulse appear at the $f = 9.8$ MHz modulation frequency of the pump beam and are extracted with an rf lock-in amplifier.¹⁸ The two channels of the output of the rf lock-in amplifier are then measured by a pair of audio frequency lock-in amplifiers locked to the frequency of the mechanical chopper. This double-modulation technique is needed to suppress artifacts in the data created by pump light scattered by the nanoparticles and improve the signal-to-noise ratio.

Since the thermal decay times of the nanoparticles are much longer than the duration of the pump pulse and are much shorter than the oscillation period of the model-locked laser, the transient absorption measurements are relatively easily interpreted as a direct measurement of the temporal evolution of the temperature of the particle subjected to an instantaneous source of heat. An analysis of the particle temperature is, however, more easily accomplished by first solving the equations that describe the flow of heat resulting from a periodic heat source, i.e., by solving the equations in the frequency domain.

We write three equations for temperature of metal core T_p , the boundary condition on the temperature of the fluid T_f adjacent to the shell, and the temperature field in the shell. The temperature gradient within the metal core is negligible. The temperature is assumed to be continuous at the core-shell and shell-solvent boundaries; in other words, we assume that the thermal resistance of the interface is negligible.

$$\frac{4\pi}{3}i\omega r_1^3 C_p T_p = P - 4\pi r_1^2 F_1 \quad (1)$$

$$r_2^2 F_2 = T_f(1 + q_f r_2)\Lambda_f r_2 \quad (2)$$

$$rT = \alpha \exp(-q(r - r_1)) + \beta \exp(q(r - r_1)) \quad (3)$$

Here, C_p is the heat capacity per unit volume of the particle; P is the power of the heat source at frequency ω , F_1 is the heat flux at the particle-shell interface; F_2 is the heat flux at the shell-fluid interface; r_1 is the core radius; r_2 is the total core-shell radius; $1/|q|$ is the thermal diffusion length in the shell; $q^2 = i\omega C/\Lambda$ where C and Λ are the heat capacity per unit volume and thermal conductivity of the shell and $1/|q_f|$ is the thermal diffusion length in the fluid: $q_f^2 = i\omega C_f/\Lambda_f$; and C_f and Λ_f are the heat capacity per unit volume and thermal conductivity of the fluid. The terms α and β are unknown coefficients that are eliminated by the continuity of the temperature at the interfaces, $T(r_1) = T_p$ and $T(r_2) = T_f$. Thus, an analytical solution for T_p , while cumbersome, is an algebraic expression in the frequency domain.¹⁷

Since small changes in optical absorption will be a linear function of the particle temperature,¹² the in-phase signal of

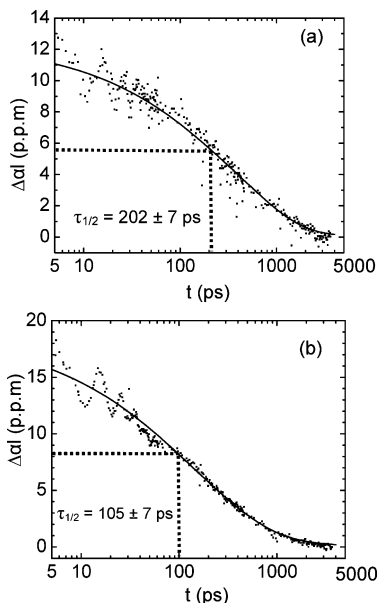


Figure 2. Data points are the measured transient changes in optical absorption for suspensions of Au-core polymer-shell nanoparticles. (a) In pure water, the best fit (solid line) gives the thermal conductivity of the shell $\Lambda_{\text{shell}} = 0.25 \pm 0.03 \text{ W m}^{-1} \text{ K}^{-1}$. $\tau_{1/2} = 202 \pm 7 \text{ ps}$. (b) In 15 vol % THF/85 vol % H_2O mixture, the best fit (solid line) gives $\Lambda_{\text{shell}} = 0.50 \pm 0.05 \text{ W m}^{-1} \text{ K}^{-1}$. $\tau_{1/2} = 105 \pm 7 \text{ ps}$. For both (a) and (b) the pump power is 15 mW and probe power is 11 mW. The sample path length $l = 0.2 \text{ mm}$ and the absorption length $\alpha^{-1} \approx 14 \text{ nm}$. The calculated thermal decays are obtained from eq 1–5.

the lock-in amplifier is¹⁹

$$S(q) = T_p(q/\tau + f) + T_p(q/\tau - f) \quad (4)$$

$$V_{\text{in}}(t) = A \sum_{q=-\infty}^{\infty} S(q) \exp(i2\pi tq/\tau) \quad (5)$$

where τ is the time between pulses, t is the time delay between pump and probe, and A is a constant.

In Figure 2a, we plot the transient change in optical absorption for Au-core polymer-shell nanoparticles in pure water. Each spectrum shows oscillations at delay times $t < 50 \text{ ps}$, superimposed on a thermal relaxation over a longer time scale. The oscillations are created by the spherically symmetric vibrational modes of the Au core. The period of these breathing modes is expected to be $\Gamma = D/(0.93v_1)$, where v_1 is the longitudinal speed of sound ($v_1 = 3240 \text{ m/s}$ for Au), and D is the diameter of the Au core.²⁰ Using the Au core diameter measured by TEM ($D = 31 \text{ nm}$), this equation predicts $\Gamma = 10.3 \text{ ps}$, in good agreement with the measured value $\Gamma \approx 9.7 \text{ ps}$.

We fit the decay of the temperature of the Au-core to the thermal model described above with two free parameters: the thermal conductivity of polymer shell and the value of the constant A that provides a scaling factor for the y-axis. All other parameters in the model are fixed; the radius of the Au core r_1 and polymer shell thickness $r_2 - r_1$ are given by TEM measurements, $C_{\text{Au}} = 2.49 \text{ J cm}^{-3} \text{ K}^{-1}$, $C_{\text{water}} = 4.18 \text{ J cm}^{-3} \text{ K}^{-1}$, $\Lambda_{\text{water}} = 0.6 \text{ W m}^{-1} \text{ K}^{-1}$, $C_{\text{polystyrene}} = 1.28$

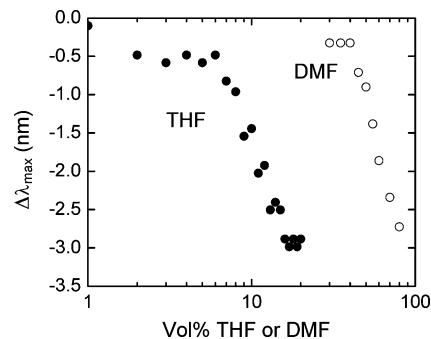


Figure 3. Shift in wavelength of the maximum plasmon absorption with the volume fraction of THF (solid circles) or DMF (open circles) in aqueous Au-core polymer-shell nanoparticle suspensions. In pure water, $\lambda = 548.8 \text{ nm}$.

$\text{J cm}^{-3} \text{ K}^{-1}$. As shown in Figure 2a, the best fit of the thermal model to the data gives $\Lambda_{\text{shell}} = 0.25 \pm 0.03 \text{ W m}^{-1} \text{ K}^{-1}$. The value is larger than $0.16\text{--}0.18 \text{ W m}^{-1} \text{ K}^{-1}$ reported in the literature for polystyrene.²¹ To provide a simple but quantitative characterization of the cooling time, we define the half-decay-time $\tau_{1/2}$ as the time required for the change in optical absorption to decay by a factor of 2 relative to the optical absorption at 5 ps; $\tau_{1/2} = 202 \pm 7 \text{ ps}$ for core-shell nanoparticles in pure water. In general, the longer time scale decay is slower than previously observed for 10 nm Pt or 20 nm AuPd nanoparticles in water where $\tau_{1/2}$ is approximately 35–50 ps.^{6,12} For 31 nm citrate-stabilized Au nanoparticles in pure water (used as Au core in the synthesis of the core-shell nanoparticles), $\tau_{1/2}$ is approximately 94 ps (data not shown).

We expected that swelling the polymer shell with organic solvent should result in minimal changes in the thermal relaxation of the core-shell nanoparticles; however, this is not the case. Figure 2b shows transient changes in optical absorption from suspensions of Au-core polymer-shell nanoparticles in a 15 vol % THF/85 vol % H_2O mixture. The decay of the temperature of the Au core is significantly faster than in the pure water ($\tau_{1/2} = 105 \pm 7 \text{ ps}$ in 15 vol % THF/85 vol % H_2O mixture) and the best fit gives a larger effective thermal conductivity of the shell ($\Lambda_{\text{shell}} \approx 0.50 \pm 0.05 \text{ W m}^{-1} \text{ K}^{-1}$).

We found a direct correlation between solvent swelling of the polymer shell and thermal relaxation of the particle core, as shown by concurrent changes in the thermal conductivity and in the surface plasmon absorption of the nanoparticles with varying solvent composition. The wavelength of maximum surface plasmon absorbance (λ_{max}) of Au nanoparticles is dictated by the refractive index of the local surrounding medium. λ_{max} is thus an indicator of solvent infiltration into the polymer shell surrounding the nanoparticle. The high index of refraction of polystyrene ($n_{\text{PS}} = 1.55$) red-shifts the surface plasmon resonance of aqueous Au-core PS-shell nanoparticles ($\lambda_{\text{max}} = 549 \text{ nm}$) relative to bare aqueous Au nanoparticles ($\lambda_{\text{max}} = 529 \text{ nm}$, $n_{\text{H}_2\text{O}} = 1.33$). Figure 3 shows the change in λ_{max} for a suspension of aqueous Au-core PS-shell nanoparticles as organic cosolvent was added to the solution. Low fractions of added cosolvent had little effect on λ_{max} , but at a critical cosolvent composition

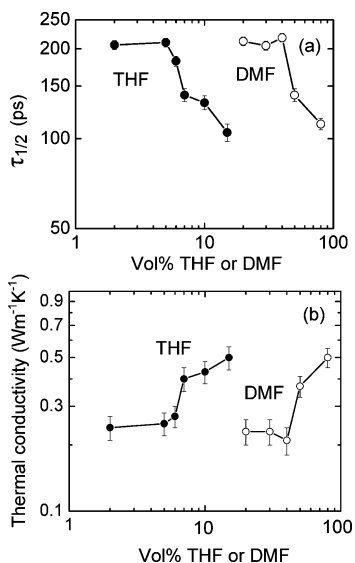


Figure 4. Changes in the (a) half decay time and (b) effective thermal conductivity of the shell with the volume fraction of THF (solid circles) and DMF (open circles) in aqueous Au-core polymer-shell nanoparticle suspensions.

(6% THF, or 40% DMF), the plasmon resonance of the particles is abruptly blue-shifted as solvent swelled the polymer shell. We attribute this sharp change in absorbance wavelength to a critical solvent composition threshold for swelling, which is consistent with past theoretical^{22,23} and experimental^{24,25} work on swelling in macroscopic polymer networks and is similar to critical swelling transitions observed in cross-linked poly(*n*-isopropyl)acrylamide gels.²⁶ The difference between the critical solvent fractions for THF and DMF is explained by the different compatibilities of these solvents for the PS shell; the Flory–Huggins solubility parameter of polystyrene ($\delta = 17\text{--}20 \text{ MPa}^{1/2}$) is closer to that of THF ($\delta = 18.6 \text{ MPa}^{1/2}$) than DMF ($\delta = 24.8 \text{ MPa}^{1/2}$), and so less THF must be added than DMF to make the solvent compatible with the PS layer.²⁷

Because the index of refraction for the water/cosolvent mixture was always less than that of polystyrene ($n_{\text{THF}} = 1.41$, $n_{\text{DMF}} = 1.43$), the particle absorbance was always blue-shifted by swelling. Since the volume of the polymer shell is nearly an order of magnitude larger than the volume of the Au core, the shift in the plasmon resonance is simply related to the index of refraction of the shell; a shift of 3 nm indicates that the index of refraction of the polymer shell has decreased by 0.03.^{17,28} If this change in index of refraction is solely due to THF penetration into the shell, the maximum volume fraction of THF in the shell would be approximately 20%; if water also contributes, because $n_{\text{water}} < n_{\text{THF}}$, then the volume fraction of solvent in the swollen shell is smaller. THF and DMF have similar refractive indices, and therefore this estimate of solvent penetration is also valid for DMF/water mixtures. These data also allow us to estimate the small changes in heat capacity and radius of the polymer shell that result from solvent penetration.¹⁷

Figure 4a shows how the half decay time $\tau_{1/2}$ changes with the volume fraction of the cosolvent. In the THF/H₂O system, $\tau_{1/2}$ decreases from 202 ps in pure water to 105 ps in 15 vol

% THF/85 vol % H₂O with a threshold near 5 vol %. In the DMF/H₂O system, the $\tau_{1/2}$ decreases from 200 ps in pure water to 107 ps in 80 vol % DMF-20 vol % H₂O with a threshold near 40 vol %. A full fit of the thermal model allows us to extract how the effective thermal conductivity of the polymer shell evolves with swelling, see Figure 4b. The thermal conductivity increases abruptly near the critical concentration of cosolvent that produces swelling and reaches a maximum of approximately $0.50 \pm 0.05 \text{ W m}^{-1} \text{ K}^{-1}$ in both THF/water and DMF/water mixtures.

These changes in the effective thermal conductivity of the shell with swelling cannot be directly attributed to solvent penetration into the shell. Water has a relatively large thermal conductivity ($0.6 \text{ W m}^{-1} \text{ K}^{-1}$), but our data for the shift in the plasmon resonance, see Figure 3, indicate that the water content of the shell must be less than 10 vol %. This small amount of water is not expected to produce a large change in the thermal conductivity of the shell. The thermal conductivity of THF ($0.14 \text{ W m}^{-1} \text{ K}^{-1}$) and DMF ($0.18 \text{ W m}^{-1} \text{ K}^{-1}$) are near the thermal conductivity of the fully collapsed PS shell, and therefore approximating the thermal properties of the swollen shell by averaging the properties of the solvent and polymer components²⁹ cannot explain the increase in the thermal conductivity of the shell.

Changes in the thermal conductivity of the shell that might be produced by enhanced alignment of the polystyrene backbone²⁷ are more difficult to rule out, but this mechanism also appears to be an unlikely explanation for our results. Experiments on drawn amorphous polymers typically show that draw ratios of 2–3 are required to produce a thermal conductivity enhancement of a factor of 2.³⁰ While swelling of the polymer shell may produce some additional stretching of the polystyrene backbone, we do not anticipate that this stretching could reach a factor of 2 in magnitude. In addition, the polymer chain is not covalently tethered to the nanoparticle surface, and thus any stretching should be minimal.

Finally, we emphasize that theoretical calculations of heat transport in nanoscale systems may not be reliable if those calculations are based on the thermal properties of bulk phases. In our experiments, the thermal conductivity of a swollen nanoscale polymer film displays a relatively large thermal conductivity. This factor of 2 increase in the thermal conductivity is unexpected and leads to factor of 2 increase in the cooling rate of the Au core.

Acknowledgment. This work was supported by U.S. DOE Grant No. DEFG02-01ER45938. The Ti:sapphire laser is part of the Laser Facility of the Seitz Materials Research Laboratory at the University of Illinois. We thank Xuan Zheng for programming the control software for the thermal measurements.

Supporting Information Available: TEM images of the nanoparticles in THF/H₂O mixture before and after dialysis with DI water; description of the analytical solution for T_p ; discussion on using shift in the wavelength of plasmon resonance to extract solvent concentration inside the shell. These materials are available free of charge via the Internet at <http://pubs.acs.org>.

References

- (1) Hamad-Schifferli, K.; Schwartz, J. J.; Santos, A. T.; Zhang, S. G.; Jacobson, J. M. *Nature* **2002**, *415*, 152–155.
- (2) Loo, C.; Lin, A.; Hirsch, L.; Lee, M. H.; Barton, J.; Halas, N.; West, J.; Drezek, R. *Technol. Cancer Res. Treat.* **2004**, *3*, 33–40.
- (3) O'Neal, D. P.; Hirsch, L. R.; Halas, N. J.; Payne, J. D.; West, J. L. *Cancer Lett.* **2004**, *209*, 171–176.
- (4) Huttmann, G.; Birngruber, R. *IEEE J. Sel. Top. Quantum* **1999**, *5*, 954–962.
- (5) Hu, M.; Hartland, G. V. *J. Phys. Chem. B* **2002**, *106*, 7029–7033.
- (6) Wilson, O. M.; Hu, X. Y.; Cahill, D. G.; Braun, P. V. *Phys. Rev. B* **2002**, *66*, 224301.
- (7) Link, S.; Furube, A.; Mohamed, M. B.; Asahi, T.; Masuhara, H.; El-Sayed, M. A. *J. Phys. Chem. B* **2002**, *106*, 945–955.
- (8) Bigot, J. Y.; Halte, V.; Merle, J. C.; Daunois, A. *Chem. Phys.* **2000**, *251*, 181–203.
- (9) Zhang, J. Z. *Acc. Chem. Res.* **1997**, *30*, 423–429.
- (10) Mohamed, M. B.; Ahmadi, T. S.; Link, S.; Braun, M.; El-Sayed, M. A. *Chem. Phys. Lett.* **2001**, *343*, 55–63.
- (11) Hu, M.; Wang, X.; Hartland, G. V.; Salgueirino-Maceira, V.; Liz-Marzan, L. M. *Chem. Phys. Lett.* **2003**, *372*, 767–772.
- (12) Ge, Z.; Cahill, D. G.; Braun, P. V. *J. Phys. Chem. B* **2004**, *108*, 18870–18875.
- (13) Kang, Y.; Taton, T. A. *Angew. Chem., Int. Ed. Engl.* **2005**, *44*, 409–412.
- (14) Huang, H. Y.; Kowalewski, T.; Remsen, E. E.; Gertzmann, R.; Wooley, K. L. *J. Am. Chem. Soc.* **1997**, *119*, 11653–11659.
- (15) Frens, G. *Nat. Phys. Sci.* **1973**, *241*, 20–22.
- (16) Kang, Y.; Taton, T. A. *J. Am. Chem. Soc.* **2003**, *125*, 5650–5651.
- (17) See Supporting Information.
- (18) O'Hara, K. E.; Hu, X. Y.; Cahill, D. G. *J. Appl. Phys.* **2001**, *90*, 4852–4858.
- (19) Cahill, D. G.; Goodson, K.; Majumdar, A. *J. Heat. Trans.* **2002**, *124*, 223–241.
- (20) Tamura, A.; Higeta, K.; Ichinokawa, T. *J. Phys. C Solid State* **1982**, *15*, 4975–4991.
- (21) Dashora, P.; Gupta, G. *Polymer* **1996**, *37*, 231–234.
- (22) Flory, P. J. *J. Chem. Phys.* **1950**, *18*, 108–111.
- (23) Iwatsubo, T.; Ogasawara, K.; Yamasaki, A.; Masuoka, T.; Mizoguchi, K. *Macromolecules* **1995**, *28*, 6579–6585.
- (24) Amiya, T.; Hirokawa, Y.; Hirose, Y.; Li, Y.; Tanaka, T. *J. Chem. Phys.* **1987**, *86*, 2375–2379.
- (25) Hirokawa, Y.; Tanaka, T. *J. Chem. Phys.* **1984**, *81*, 6379–6380.
- (26) Heskins, M.; Guillet, J. E. *J. Macromol. Sci., Chem.* **1968**, *2*, 1441–1455.
- (27) Zhang, L. F.; Eisenberg, A. *Polym. Adv. Technol.* **1998**, *9*, 677–699.
- (28) Mulvaney, P.; Liz-Marzan, L. M.; Giersig, M.; Ung, T. *J. Mater. Chem.* **2000**, *10*, 1259–1270.
- (29) Li, C. C. *AIChE J.* **1976**, *22*, 927–930.
- (30) Choy, C. L.; Wong, Y. W.; Lau, K. W. E.; Yang, G. W.; Yee, A. F. *J. Polym. Sci. Pol. Phys.* **1995**, *33*, 2055–2064.

NL047944X